We are IntechOpen, the world's leading publisher of Open Access books
Built by scientists, for scientists

3,700
Open access books available

108,500
International authors and editors

1.7 M
Downloads

Our authors are among the

154
Countries delivered to

TOP 1%
most cited scientists

12.2%
Contributors from top 500 universities

CLARIVATE ANALYTICS
BOOK CITATION INDEX
INDEXED

WEB OF SCIENCE™

Selection of our books indexed in the Book Citation Index in Web of Science™ Core Collection (BKCI)

Interested in publishing with us?
Contact book.department@intechopen.com

Numbers displayed above are based on latest data collected.
For more information visit www.intechopen.com

21

Remote Characterization of Microwave Networks - Principles and Applications

Somnath Mukherjee
RB Technology
USA

1. Introduction

The present work deals with characterization of RF/Microwave one-port networks remotely, i.e. without any wired connections between the Device under Test (DUT) and the measuring apparatus. The objective is a frequency domain characterization of the complex reflection coefficient (or complex impedance) of the one-port so that its equivalent circuit model may be constructed. Finally, applications of this technique to ultra low-cost sensors and Radio Frequency Identification Devices (RFID) will be outlined

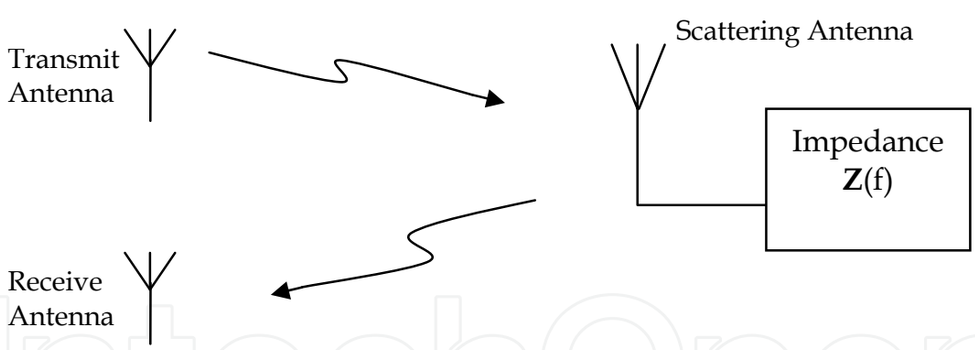

Fig. 1. Scattering Antenna in Bistatic Mode

Fig.1 diagrammatically depicts the problem, where the one-port under test, represented by the impedance **Z**(f) is used as a termination for the so-called Scattering Antenna. The Transmit Antenna is a part of the measurement system and is used to illuminate the Scattering Antenna with RF energy. The backscatter from the Scattering Antenna is received by the Receive Antenna – again part of the measurement system. The objective is to recover the frequency dependent complex impedance **Z**(f) by processing the backscatter. Fig. 1 illustrates the measurement in a bistatic arrangement, though monostatic implementations may be considered if necessary.
We would like to point out that the scattering antenna and the one-port may be devoid of any active electronics, including means to convert RF energy to DC.

If $\mathbf{Z}_A$ is the impedance of the scattering antenna at the point where the unknown one-port $\mathbf{Z}(f)$ is connected, then the reflection coefficient $\Gamma(f)$ at the scattering antenna terminals is

$$\Gamma(f) = \frac{\mathbf{Z}(f) - \mathbf{Z}_A}{\mathbf{Z}(f) + \mathbf{Z}_A} \tag{1}$$

For the special case of Z(f) being lossless (= X(f)) and $\mathbf{Z}_A$ being resistive (=R_A) , we have

$$|\Gamma(f)| = 1 \tag{2a}$$

and,

$$\Gamma(f) = 1.\arg(\Gamma(f)) = -2\arctan(X(f)/R_A) \tag{2b}$$

Therefore, the task of characterizing $\mathbf{Z}(f)$ (i.e. $\Gamma(f)$) for a lossless one-port reduces to characterizing the phase-frequency profile of its reflection coefficient.

The fundamental advantage of frequency domain characterization is the ability to cover a large RF bandwidth while maintaining a narrow detection bandwidth, resulting in a favorable Carrier to Noise ratio (CNR). Furthermore, use of a large RF bandwidth enables spatial resolution of 'targets' – the theoretical limit to such resolution given by c/2B where c = speed of light, B = Bandwidth of the illuminating signal (Ulaby et al., 1982). The above principle behind spatial resolution is general and independent of the type of waveform. Ultra-wide band (UWB) radar is therefore attractive due to its ability to provide fine resolution, in addition to its robustness against multi-path and narrow-band interference (Yarovoy 2007).

Frequency domain measurements in bounded medium are routinely performed using a Vector Network Analyzer (VNA) and one is tempted to use the same for remote measurement as well. Use of VNA for polarimetric scattering measurements has been documented extensively such as (Ulaby et al., 1990). Such instruments have been extensively used to characterize ground, sea-ice and similar natural objects.

The present discussion is focused on the remote characterization of synthetic targets (i.e. a scattering antenna terminated by one-port) by coherent processing of backscatter – with applications to sensors and RFID. For such applications, the probing platform ('Reader') needs to be priced economically, as well be capable of functioning in presence of clutter and multipath. The transmit and the receive antennas are more often than not collocated, and therefore significant carrier leakage exist between the two. The above undesired phenomena termed impairments need to be addressed in a successful measurement scheme.

2. Scattering Antennas

The present section outlines the type of antennas suitable for remote measurement of one-port networks.

2.1 Salient Features of Scattering Antennas

When $\mathbf{Z}(f)$ in Fig.1 is lossless, intuitively speaking, all the power captured by the antenna should be re-radiated back as no energy is dissipated in the terminating reactance. Therefore, as described by eqn. 2(a) and (b), the scattering antenna should scatter back the same power irrespective of the type of lossless termination (including open and short), as

they all produce a reflection coefficient of unity and therefore the radar cross-section (RCS) should be ideally constant. However, a counter-example in the form of 'minimum-scatter antennas' (Kahn 1965, Nikitin 2006) where no power is scattered back under open circuited condition demands further investigation. A typical example of 'minimum-scatter antennas' is the one-dimensional dipole without parasitic elements, where no current flows under open circuit condition when illuminated with RF energy, and RCS tends to disappear.

A Thevenin/Norton equivalent circuit is traditionally used to model antennas in transmit and receive modes (Balanis 1982). According to that model, under matched conditions, a receive antenna scatters back as much power as absorbed by the load. The limitations to that model have been discussed in several references such as Andersen 2003, Colin 2003, Pozar 2004, and in general, the model is not valid to interpret scattering related questions. The limitation is obvious for antennas containing parasitic elements, where the RCS might approach zero under matched conditions (Pozar 2004).

Let us now summarize some desirable characteristics of a scattering antenna.

1. Obviously, a 'minimum scatter antenna' is not a suitable candidate as RCS approaches zero under open circuit conditions.
2. It is important to realize the limitation of Thevenin/Norton model to study scattering by antennas that are not 'minimum scatter'.
3. The concept of antenna aperture may not be relevant as ideally no power is absorbed in a lossless termination. Complex RCS (equation (6)) appears to be a more suitable metric.
4. The physical mechanism through which an antenna absorbs power from an incident wave is destructive interference, i.e. the antenna scatters so as to cancel some of the incident fields (Kahn 1965). Ideally we would prefer no 'structural scattering' (Nikitin 2006, Hansen 1989) from a scattering antenna, i.e. no scattering when the said antenna is terminated by a matched load. This ensures that the energy incident on the antenna travels in its entirety to the terminal reactance and eventually gets reflected and re-radiated. Antennas with parasitic or passive elements have the potential to reach zero structural scattering (Pozar 2004) and can scatter even when the active element is open circuited (Andersen 2003), making them attractive as scattering antennas.

2.2 Two-port Representation of Scattering Antennas

Let us consider a Scattering Antenna operating in bistatic mode as in Fig.1. We propose that a non-minimum scattering antenna can be modeled as a simple two-port network (Fig.2) whose parameters can be extracted using traditional Vector Network measurement techniques. We assume far-field behavior throughout.

The incident wave from the transmit antenna **a** is modeled as coming from a generator of impedance Z0 where Z0= impedance of free space (120π). $\gamma l1$ represent the forward propagation coefficient from the Transmit Antenna to the Scattering Antenna, and $\gamma l2$ the return propagation coefficient from the Scattering Antenna to the Receive Antenna. The scattered wave **b** is generated due to reflection from the equivalent two-port network terminated by the unknown one-port network Γ (DUT). The objective is to de-embed the effect of the two-port network "error" network and determine Γ. In other words, this ensures characterizing the DUT alone, minus the effect of the antenna.

As discussed in section 2.1, a certain class of antennas terminated by a matched load results in low RCS. This phenomenon occurs only when the antenna is resonant, i.e. capable of radiating power in the transmit mode. Outside resonance, the antenna radiates negligible

power in transmit mode, and scatters back finite energy even when terminated by the

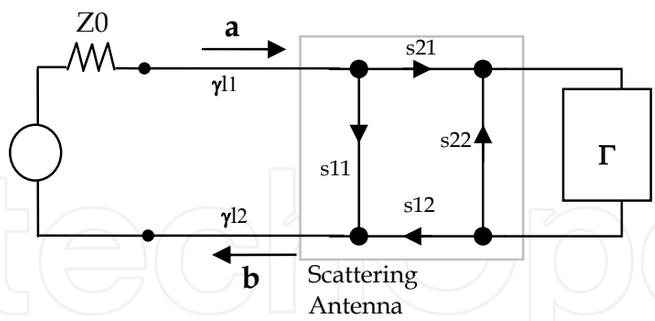

Fig. 2. Scattering Antenna modeled as a 2-port

characteristic impedance, most of the backscatter energy coming from "structural" scattering. As a result, the unknown one-port **Γ** will have negligible effect on the backscatter under these conditions. Therefore, under resonant condition, **s**11 in Fig.2 is expected to become small, and outside resonance, |**s**11| may even approach unity. **s**11 is therefore an important figure of merit to quantify structural scattering.

2.3 Example of Two-port Representation of a Scattering Antenna

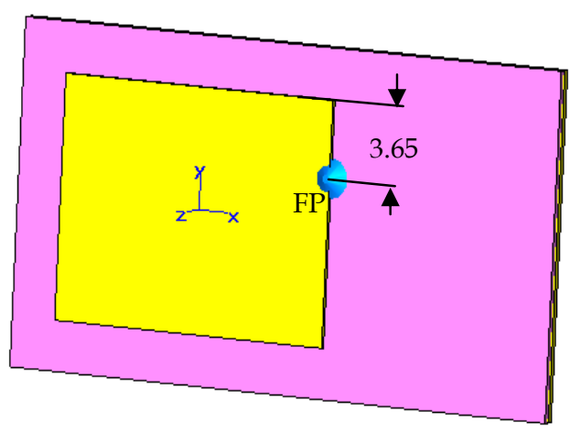

Fig. 3. Rectangular Microstrip Patch used as Scattering Antenna

A microstrip patch satisfies the requirements listed in Section 2.1, and was therefore considered a candidate for a scattering antenna. Simulation using commercially available Electromagnetic Simulator (CST Microwave Studio 2008 from Computer Simulation Technology) was tried on a rectangular patch on a finite ground as shown in Fig.3. The patch had dimensions of 11.5 X 15 mm and mounted on a ground plane 16.3 X 30 mm maintaining symmetry in the Y-direction. The ground plane was intentionally made larger in the X-direction than necessary to create 'structural scattering' or 'clutter'. Copper was selected as the conducting material for both ground plane and the patch, whereas the substrate was assumed lossless with a permittivity (ε_r) of 4.5. The thickness of the substrate was 0.8 mm. A feed point (FP), located 3.65 mm below the longer edge (Fig.3), was used to

connect various one-port networks. The impedance at FP happened to be 50Ω, though feed points with other impedance levels could be used. Typical one-port networks used were open, short, termination (50Ω), lumped inductors and capacitors.

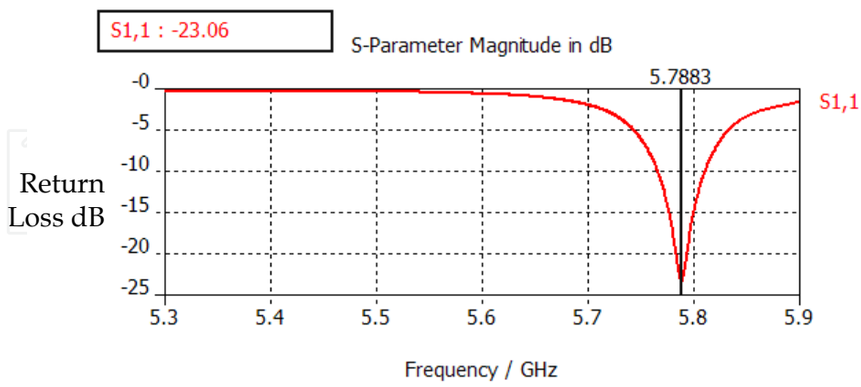

Fig. 4. Return Loss at FP in Transmit Mode

An approximate analysis (Balanis 1982) predicts the fundamental resonant frequencies of the patch to be 4.56 and 6.15 GHz. To investigate the scattering phenomenon, we decided to operate around the higher resonant frequency, i.e. when the longer sides are radiating and FP is located on a non-radiating edge. The non-radiating edge was selected as feed point so as to disturb the radiating field as little as possible. Simulation found the resonance to be close to 5.8 GHz in radiating mode (Fig.4), as depicted in the Return Loss at FP referenced to 50Ω. To investigate scattering, the patch was illuminated with linearly polarized wave parallel to Y-axis (Fig.3) traveling in negative Z-direction and the co-polarized backscatter was observed.

The scattered electric field vector **E**, under far-field conditions, at co-ordinates (r,θ,ϕ) can be expressed as:

$$\mathbf{E}(r,\theta,\phi) = \mathbf{e}(\theta,\phi).\ \exp(-j\beta r)/r \tag{3}$$

where β is the propagation constant.

The magnitude of RCS is defined as:

$$\sigma(\theta_i,\phi_i,\theta,\phi) = 4.\pi.[|\mathbf{e}(\theta,\phi)|^2/\ |\mathbf{E}_i(\theta_i,\phi_i)|^2] \tag{4}$$

where $\mathbf{E}_i(\theta_i,\ \phi_i)$ is the incident electric field vector in the θ_i,ϕ_i direction. Phase of the scattered field, using a convenient reference point (r = 1 meter was used in the simulation) can be expressed as

$$\Psi(\theta_i,\phi_i,\theta,\phi) = \arg[\mathbf{e}(\theta,\phi)/\ \mathbf{E}_i(\theta_i,\phi_i)] \tag{5}$$

Based on (4) and (5), we define a complex reflection coefficient as (Mukherjee 2008):

$$\Gamma(\theta_i,\phi_i,\theta,\phi) = \sqrt{\sigma(\theta_i,\phi_i,\theta,\phi)}.e^{i\Psi(\theta_i,\phi_i,\theta,\phi)} \tag{6}$$

The patch was successively terminated with an open (no termination), short and 50Ω termination at FP, and the magnitude and phase of the co-polarized **Γ** as defined by (6) were computed (Please note this **Γ** is different from one in Fig.2). Let **Γ**o, **Γ**s and **Γ**l be the

complex reflection coefficient as defined in (6) due to open, short and load conditions for $\theta=\theta_t=0$ and $\phi=\phi_t=0$. The incident and backscatter waves are in negative and positive z-direction respectively, i.e. under bore-sight conditions. It was observed that $|\Gamma l|$ is significantly lower in the middle of the band compared to $|\Gamma s|$ and $|\Gamma o|$, indicating high amount of absorption by the termination resistor (Mukherjee 2008).
The following equations were used to calculate the parameters of the error network of Fig.1 from the calibration data, viz. Γo, Γs and Γl.

$$\gamma l1.\gamma l2.\mathbf{s}11 = \Gamma l \tag{7}$$

$$\mathbf{s}22 = (\Gamma o + \Gamma s - 2.\gamma l1.\gamma l2.\mathbf{s}11)/(\Gamma o - \Gamma s) \tag{8}$$

$$\gamma l1.\gamma l2.s21.\mathbf{s}12 = (1-s22).(\Gamma o - \gamma l1.\gamma l2.\mathbf{s}11) \tag{9}$$

We note that **s**11 and **s**21.**s**12 occur de-normalized in conjunction with the term $\gamma l1.\gamma l2$.

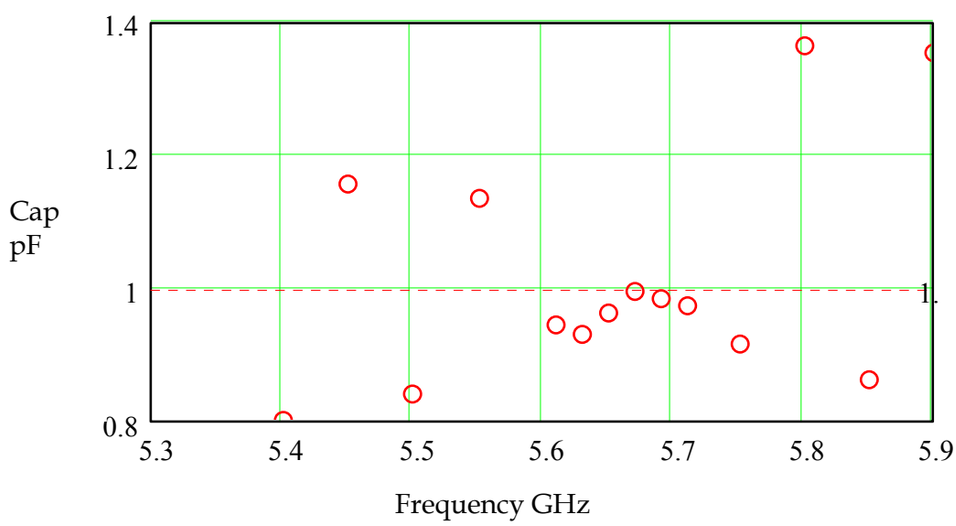

Fig. 5. De-embedded value of DUT (1 pF capacitor)

For an unknown one-port producing a backscattered reflection coefficient Γ, the de-embedded value of reflection coefficient of the DUT itself can be calculated according to

$$\Gamma corr = [\Gamma - \gamma l1.\gamma l2.\mathbf{s}11]/[\gamma l1.\gamma l2.\mathbf{s}21.\mathbf{s}12 + s22.(\Gamma - 1)] \tag{10}$$

Fig.5 shows the results of de-embedding the effect of scattering antenna (using eqn. (7), (8), (9),(10)) for a 1 pF lumped capacitor as DUT. In the vicinity of resonance, we find good agreement between the actual and the de-embedded values. However, as one moves away from resonance, the accuracy falls due to increase of structural scattering (increase in **s**11 in the two-port representation of Fig.2). The simulation assumed negligible contribution from noise.
It is worth mentioning that the backscatter measured at angles away from bore-sight also allows determining the unknown device making the approach aspect independent within certain limits.

3. Measurement Technique

The practical applications of the present technique viz. in the RFID and sensors often require the probing platform to be low cost and portable; as a result, the transmit and receive antennas may need to be co-located. This brings forth the problem of detecting a backscatter signal in the same order of magnitude or lower than the leakage between the transmit and receive antennas. RFID devices containing chips solve this problem (Dobkin 2007) by generating a subcarrier at the tag level. Since chipless devices cannot afford that luxury, one has to resort to alternative probing methods. We present here a technique suggested by Mukherjee 2007.

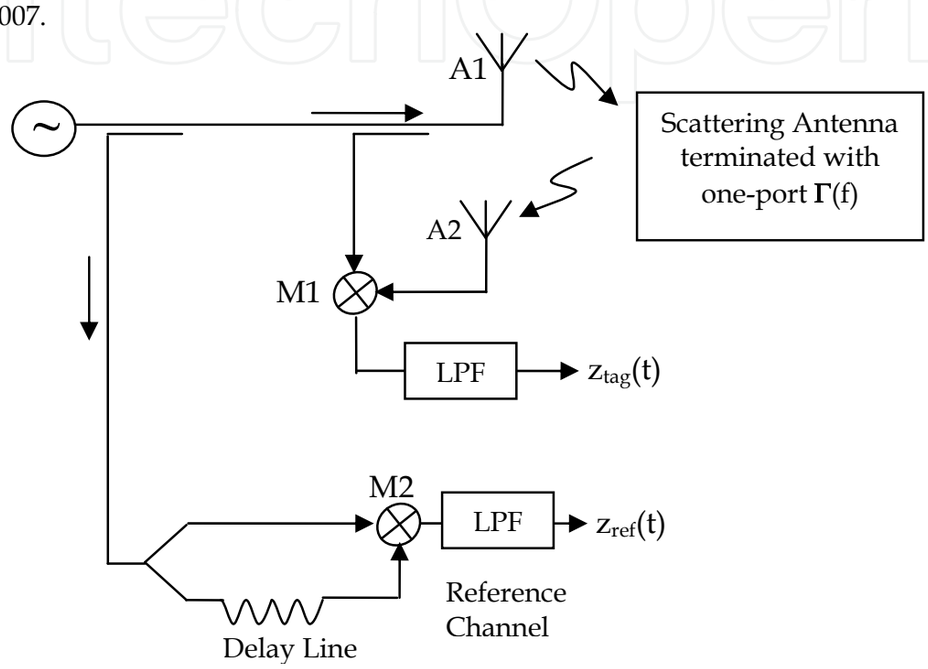

Fig. 6. Remote Measurement of Impedance

The technique bears a superficial similarity to the FMCW radar (Ulaby1982). A source generates a chirp signal that is radiated by the antenna A1 (Fig.6) to illuminate the 'target' (scattering antenna terminated by the unknown one-port $\Gamma(f)$), and another antenna A2 receives the backscattered signal. The transmitted and received signals are mixed by a mixer M1 and lowpass filtered (LPF) to generate the Intermediate Frequency (IF) signal $z_{tag}(t)$. The backscatter from the scattering antenna can be resolved spatially from the carrier leakage by filtering the IF signal. Henceforth, we consider the IF signal due to the scattering antenna only.

Simultaneously, internal to the Reader, a sample of the transmit signal is mixed with a delayed version of itself and lowpass filtered to generate a reference signal $z_{ref}(t)$.

The transmitted chirp signal can be expressed as (Brunfeldt 1991):

$$x(t) = a(t).\cos[2\pi f_0 t + K\int_0^t s(t)dt] \tag{11}$$

where a(t) is the incidental amplitude modulation of the source, and s(t) is the frequency modulating signal which is linear for a linear chirp. The instantaneous frequency f(t) is given by:

$$f(t) = f_0 + \frac{K}{2\pi}.s(t) \tag{12}$$

where f_0 is the start frequency.
The backscattered signal received at the Reader can be expressed as:

$$y(t) = L.\Gamma(f(t-\tau)).a(t-\tau).\cos\left[2\pi f_0(t-\tau) + K.\int_0^{t-\tau} s(t)dt + \psi(f(t-\tau))\right] \tag{13}$$

where τ is the round trip delay and L is the total loss (assumed constant over the frequency band), between antennas A1 and A2 through the scattering antenna.

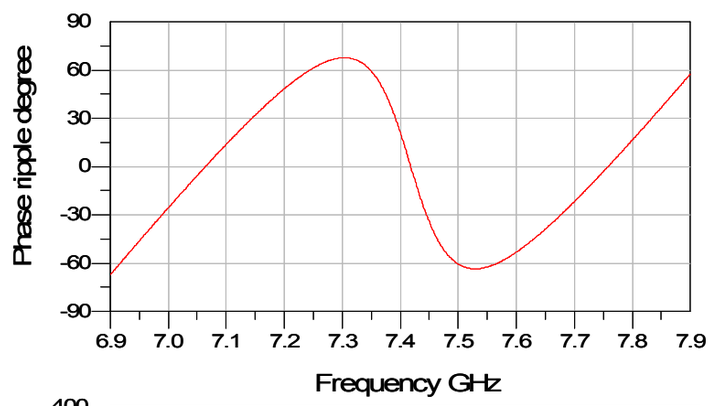

Fig. 7(a)

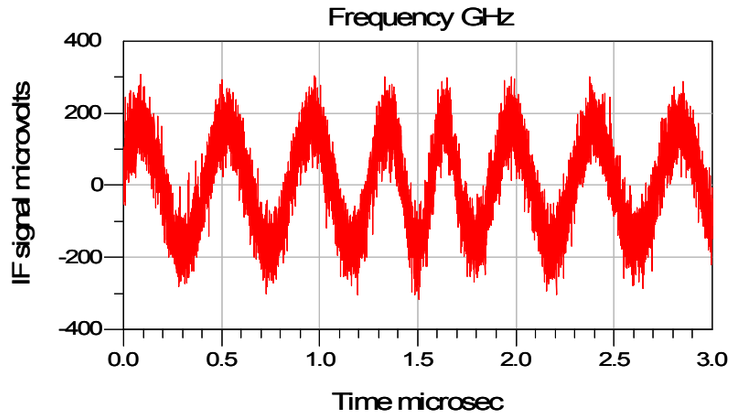

Fig. 7(b)

Fig. 7. (a) Phase Ripple of $\Gamma(f)$
Fig. 7. (b) Time Domain IF Waveform Depicting Phase Modulation

The output from the mixer M1, after filtering, can be approximated as:

$$z_{tag}(t) \approx \tfrac{1}{2}.L.a^2(t).\Gamma(f(t)).\cos[2\pi f_0\tau + K\tau.s(t) + \psi(f(t))] \tag{14}$$

provided the delay τ is small compared to the chirp duration.
For the special case of a linear chirp, (14) becomes:

$$z_{tag}(t) \cong ½.L.a^2(t).\Gamma(f(t)).\cos[2\pi f_0\tau + K\tau.t + \psi(f(t))] \quad (15)$$

The IF signal in such a case is a nominal sine wave with frequency

$$K\tau/2\pi =(B/T_R).\tau \quad (16)$$

where B = chirp bandwidth and T_R = chirp duration
The IF is thus a modulated sine wave of "carrier frequency" $(B/T_R).\tau$ together with amplitude and phase modulation according to $\Gamma(f(t))$. In other words, a mapping occurs for the complex function $\Gamma(f)$ from the frequency to time domain. Therefore, demodulation of the IF signal in (15) should provide information on the reflection coefficient between frequencies f_0 and f_0 + B.
Fig.7(b) represents $z_{tag}(t)$ as generated by simulation with the following parameters:
f_0 = 6.9 GHz, B=1 GHz, T_R= 3 μs with a round trip delay τ produced by propagation through 2 meters in air (i.e.1 meter in each direction). $\Gamma(f)$ was chosen to be a lossless one-port with a phase-frequency profile as in Fig.7(a).
It is interesting to observe the correlation in phase modulation in Fig.7(b) with the phase ripple of $\Gamma(f)$ in Fig.7(a).
The task of recovering the phase ripple of $\Gamma(f)$ (magnitude being unity) could be achieved through the use of the Reference Channel in Fig.6.
Following the same procedure as above, we have:

$$z_{ref}(t) \cong ½.L_{ref}.a^2(t).\cos[2\pi f_0\tau_{ref} + K\tau_{ref}.t + \psi_{ref}] \quad (17)$$

where τ_{ref} is the delay in the reference channel.
We have made the reasonable assumption that the loss L_{ref} and phase shift ψ_{ref} in the reference channel are independent of frequency.
Each of the equations (15) and (17) can be converted from real time functions to complex time functions by application of Hilbert Transform. The complex functions can be expressed as:

$$\zeta tag(t) = ½.L.a^2(t).\Gamma(f(t)).\exp\{j[2\pi f_0\tau + K\tau.t + \psi(f(t))]\} \quad (18a)$$
$$\zeta ref\ (t) = ½.L_{ref}.a^2(t).\exp\{j[2\pi f_0\tau_{ref} + K\tau_{ref}.t + \psi_{ref}]\} \quad (18b)$$

Therefore,

$$\arg(\zeta tag(t)/\ \zeta ref(t)) = 2\pi f_0.(\tau-\tau_{ref}) + K.(\tau- \tau_{ref}).t + \psi(f(t)) + \psi_{ref} \quad (19)$$

We are usually interested in the phase ripple $\psi(f(t))$ and therefore the first and fourth terms in the right hand side of (19) can be scaled out. The second term indicates a linearly progressive phase shift with frequency that can be conveniently factored out by unwrapping the phase. Therefore, the desired phase ripple $\psi(f(t))$ can be determined.

There could be alternative ways to recover the phase ripple information and this method is not claimed to be the optimum one.
We observe that the detection bandwidth in the method as in Section 3 can be made sufficiently small as to reduce the thermal noise – while operating with large RF bandwidth at the same time.
The approach is essentially a broadband technique and therefore carries its usual advantages. Moreover, it need not operate over a continuous spectrum of frequencies – as it could maintain phase coherence in the reader while selectively shutting off parts of the chirp in time.

4. Applications

The present section will outline some applications of the remote measurement of impedance to RFID and sensors. The RFID would use the one-port as a vehicle for storing the coded information. And, a remotely monitored sensor could be constructed by utilizing a one-port that gets predictably affected by a physical parameter such as temperature, pressure, strain, magnetic field etc. In either case, they would operate without DC power (including one generated by a rectifying antenna) and be free of semiconductor components. This opens up the possibility of printed RF barcodes (with conducting ink on low-cost substrate such as paper or plastic) and disposable sensors. This approach has the potential to reduce the cost by orders of magnitude compared to existing technology including printed electronics.
Such devices should have a longer range compared to those utilizing rectifying antenna, where a significant fraction of the received RF power is converted to DC to operate the associated electronics. On the other hand, the chipless devices being designed lossless (ideally), could potentially re-radiate all the received power.

4.1 Application to RFID

Section 3 demonstrated that it is possible to recover remotely the phase-frequency profile of an unknown reactance (one-port) connected to an antenna port. And, we know that such phase-frequency profile is completely characterized by the poles and zeros of the one-port. With this background, we propose creation of multiple tag signatures by suitable placement of poles and zeros. As all information about the reactive network is embedded in the poles and zeros, identifying them identifies the network uniquely. The following discussion is an attempt to estimate a lower bound on the number of bits that can be encoded using this technique.
To start with, let us consider a pair consisting of a pole and zero as shown in Fig. 8 located inside a segment of bandwidth with start and stop frequencies f1 and f2. We are allowed to move the positions of poles and zeros within that segment following certain rules, and thereby calculate the number of distinct permissible states to ascertain the number of unique identification signatures.

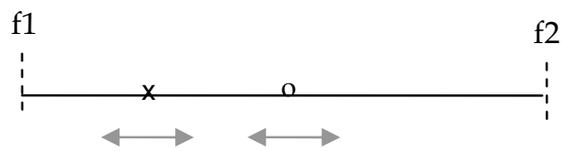

Fig. 8. Positioning of Poles and Zeros

The following rules are defined:

1. The minimum separation between a pole and its companion zero is θ. This separation is dictated by the quality factor (Q) of the resonators in the reactive network.
2. Poles or zeros can be moved in steps of ≥ Δp as dictated by measurement accuracy in presence of noise and various impairments.

To start with, let the pole be placed at f = f1 and the zero at f= f1+θ.
Next, the zero starts its journey from f1+θ and travels up to f2-θ in increments of Δp.
The i-th position of the zero is described as

$$f_i = f1 + \theta + i.\Delta p \tag{20a}$$

where i = 0…..N with

$$N = \frac{f2 - f1 - 2\theta}{\Delta p} \tag{20b}$$

Now, corresponding to the i-th position of the zero, the pole could start its journey at f1 in steps of Δp and commence at (f_i-θ).
Therefore, number of states the zero can assume for the i-th position of the pole is given by

$$\frac{f_i - \theta - f1}{\Delta p} \tag{21}$$

And, therefore corresponding to all the positions of the zero, the total number of pole-zero combinations is given by

$$\sum_{i=0}^{N} \frac{f_i - \theta - f1}{\Delta p} \tag{22}$$

Using (20a) and (20b), (22) is simplified to

$$\frac{(f2 - f1 - \theta).(f2 - f1 - \theta + \Delta p)}{2.\Delta p^2} \tag{23}$$

Now, the above exercise can be repeated for a scenario where the frequency of pole exceeds that of zero, and would generate an identical number of states. Therefore, the total number of states is given by

$$\Theta_{single} = \frac{(f2 - f1 - \theta).(f2 - f1 - \theta + \Delta p)}{\Delta p^2} \tag{24}$$

where the subscript 'single' implies number of states calculated over a single segment of bandwidth, viz. between f1 and f2 for a pole-zero pair.
Now, let us consider 'm' number of identical bandwidth segments following the same rules of positioning of poles and zeros. The total number of states can be given by

$$\Theta_m = \left(\frac{(f2 - f1 - \theta).(f2 - f1 - \theta + \Delta p)}{\Delta p^2} \right)^m \tag{25}$$

In deriving the above expression, we made some simplifying assumptions that did not account for some additional states as follows:
Each bandwidth segment always contained a pole zero pair. However, valid states are possible with just a single pole (zero) or none at all is present in a particular segment. The missing poles (zeros) could have migrated to other segments.
For a given total available bandwidth, i.e. m.(f2-f1), presence of m pole-zero pairs were assumed. However, additional states can be considered to be generated by single pair, double pair up to (m-1) pairs inhabiting the total available bandwidth. However, the number of states generated by pole zero pairs <m will be small compared to that generated from m pairs.
With the above premises, we can conclude that the number of encoded bits B is given by

$$B > \log_2(\Theta_m) \tag{26}$$

As an example, let us consider a total bandwidth of 3 GHz divided into 6 segments. Therefore, f2-f1= 500 MHz and m = 6. Let us further assume that θ =100 MHz and Δp = 25 MHz. This results in B > 48 bits, a number comparable with information content available from optical bar codes.

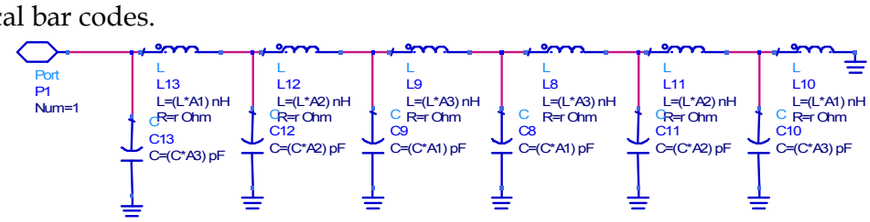

Fig. 9(a)

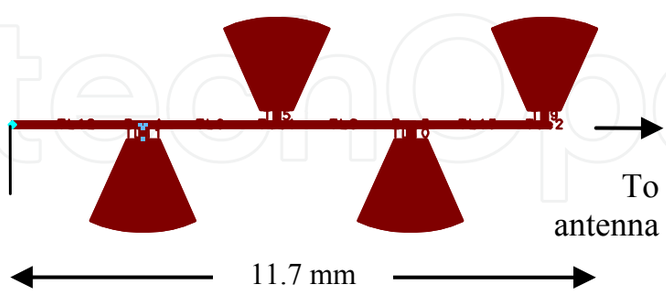

Fig. 9(b)

Fig. 9.(a) Example of Lumped Equivalent Circuit for X(f)
Fig. 9.(b) Microstrip Implementation of L-C Ladder

4.1.1 L-C Ladder as One-port

An example of the reactive one-port is a L-C ladder circuit as shown in Fig. 9(a), with its

corresponding microstrip implementation – amenable to printing technique - in Fig. 9(b). The scattering antenna – not shown in Fig. 9(b) – need to possess properties outlined in Section 2.1. The narrow lines (Fig. 9(b)) represent the series inductors and the stubs work as shunt capacitors. By changing the values of these elements, the poles and zeros can be controlled as in Section 4.1 to generate RFID information bits.

4.1.2 Stacked Microstrip Patches as Scattering Structure

While the previous discussions premised on the separation of the scattering antenna and the one-port, we now present an example where the scattering structure does not require a distinguishable one-port.

Fig. 10. depicts a set of three (there could be more) stacked rectangular patches as a scattering structure where the upper patch resonates at a frequency higher than the middle patch. When the upper patch is resonant, the middle patch acts as a ground plane. Similarly, when the middle patch is resonant, the bottom patch acts as a ground plane (Bancroft 2004).

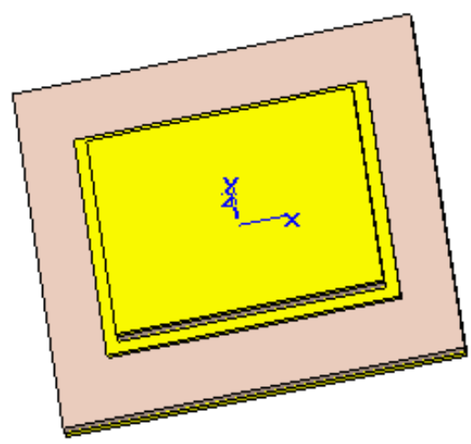

Fig. 10(a)

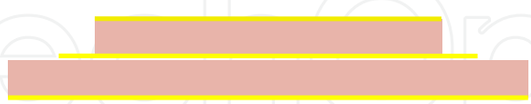

Fig. 10(b)

Fig. 10. (a) Stacked Rectangular Patches as Scattering Structure – Isometric
Fig. 10. (b) Stacked Rectangular Patches as Scattering Structure – Elevation

If the patches are perfectly conducting and the dielectric material is lossless, the magnitude of the RCS of the above structure could stay nominally fixed over a significant frequency range. As the frequency is swept between resonances, the structural scattering tends to maintain the RCS relatively constant over frequency – and therefore is not a reliable parameter for coding information. However, the phase (and therefore delay) undergoes significant changes at resonances. Fig. 11(a) and 11(b) illustrates this from simulation on the structure of Fig.10 (b). The simulation assumed patches to be of copper with conductivity

5.8. 10^7 S/m and the intervening medium had a dielectric constant =4.5 with loss tangent = 0.002. As a result of the losses, we see dips in amplitude at the resonance points.
Just like networks can be specified in terms of poles and zeros, it has been shown by numerous workers that the backscatter can be defined in terms of complex natural resonances (e.g. Chauveau 2007). These complex natural resonances (i.e. poles and zeros) will depend on parameters like patch dimension and dielectric constant. As a result, the principle of poles and zeros to encode information may be applied to this type of structure as well. However, being a multi-layer structure, the printing process may be more expensive than single layer (with ground plane) structures as in Fig. 9(b).

4.2 Application to Sensors

The principle of remote measurement of impedance could be used to convert a physical parameter (e.g. temperature, strain etc.) directly to quantifiable RF backscatter. As this method precludes the use of semi-conductor based electronics, it could be used in hazardous environments such as high temperature environment or for highly dense low cost sensors in Structural Health Monitoring (SHM) applications.

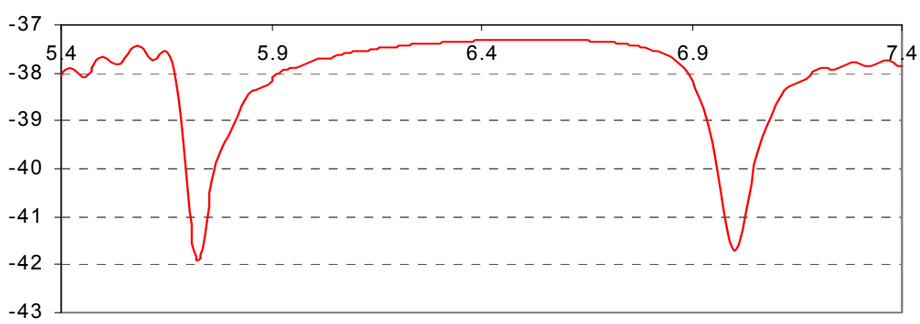

Fig. 11 (a)

Frequency GHz →

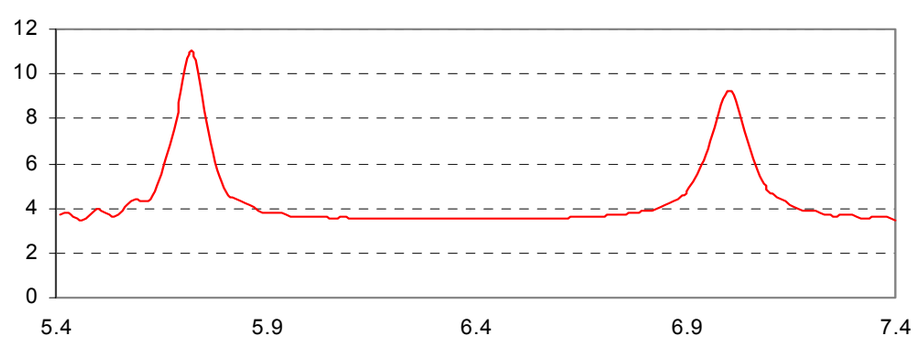

Fig. 11 (b)

Fig. 11. (a) Magnitude of Backscatter (dBV/m) from structure of Fig. 10 (a)
Fig. 11. (b) Group Delay (ns) of Backscatter from structure of Fig. 10 (a)

As an example, a temperature sensor using stacked microstrip patch has been proposed by

Mukherjee 2009. The space between a pair of patches could be constructed of temperature sensitive dielectric material whereas between the other pair could be of zero or opposite temperature coefficient. Fig.12 illustrates the movement of resonance peak in group delay for about 2.2% change in dielectric constant due to temperature.
Other types of sensors, such as strain gauge for SHM are under development.

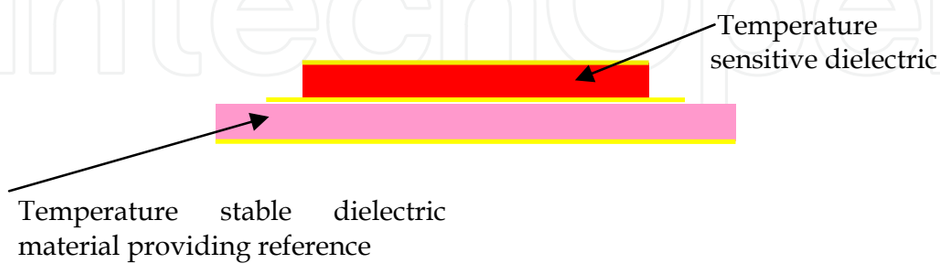

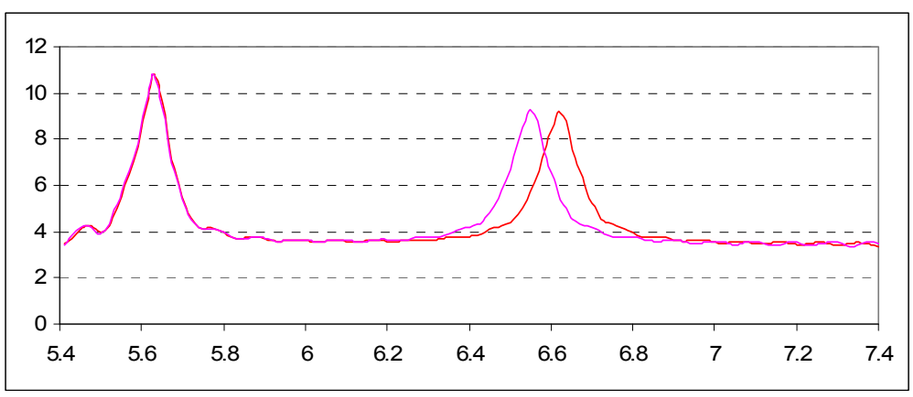

Fig. 12. Change in higher frequency resonance due to 2.2% change in ε_r

5. Impairment Mitigation

Cause of impairment is due to multipath and backscatter from extraneous objects – loosely termed clutter. The boundary between multipath and clutter is often vague, and so the term impairment seems to be appropriate. Mitigation of impairment is especially difficult in the present situation as there is no electronics in the scatterer to create useful differentiators like subcarrier, non-linearity etc. that separates the target from impairments. Impairment mitigation becomes of paramount importance when characterizing devices in a cluster of devices or in a shadowed region.
Fig. 13 illustrates with simulation data how impairments corrupt useful information. The example used the scatterer of Fig. 10 with associated clutter from a reflecting backplane, dielectric cylinder etc.
To mitigate the effect of impairments, we propose using a target scatterer with constant RCS but useful information in phase only (analogous to all-pass networks in circuits). In other words, the goal is to phase modulate the complex RCS in frequency domain while keeping

the amplitude constant. The 'modulating signal' is the information content for RFID or sensors – as the case may be. A lossless stacked microstrip patch has poles and zeros that are mirror images about the jω axis. When loss is added to the scatterer, the symmetry about jω axis is disturbed. Fig.14 illustrates the poles and zeros for the lossy scatterer described in Fig.10. The poles and zeros are not exactly mirror image about jω axis due to losses but close enough for identification purposes as long as certain minimum Q is maintained. We hypothesize that poles and zeros due to impairments will in general not follow this 'all-pass' property and therefore be distinguishable from target scatterers. Investigation using genetic algorithm is underway to substantiate this hypothesis. And, while the complex natural resonances from the impairments could be aspect dependent, the ones from the target will in general not be (Baev 2003).

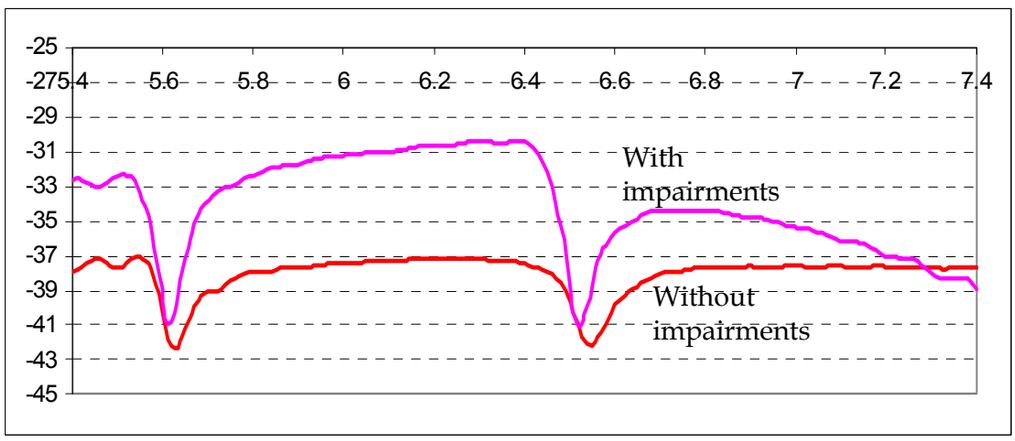

Fig. 13(a)

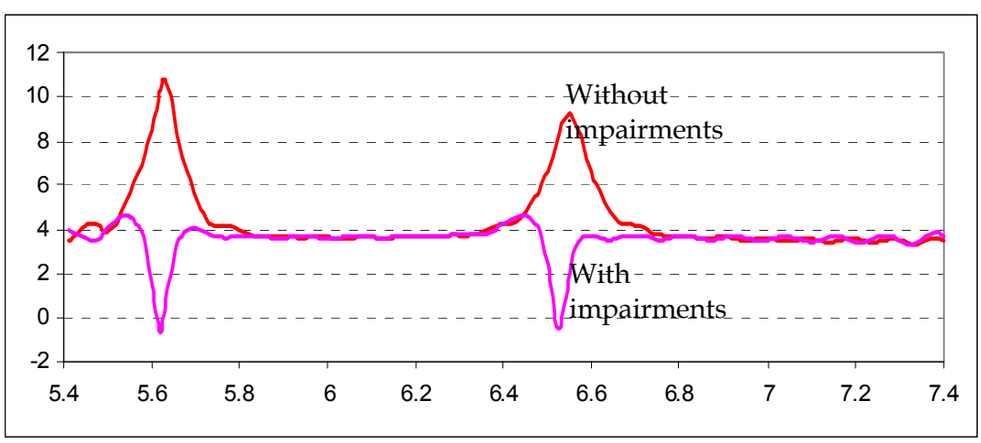

Fig. 13(b)

Fig. 13. (a) Magnitude of Backscatter (dBV/m) with and without impairments
Fig. 13. (b) Group Delay (ns) of Backscatter with and without impairments

6. Summary and Outlook

Several novel ideas have been introduced in this work - the foundation being remotely determining the complex impedance of a one-port. The above approach is next used for the development of chipless RFID and sensors. The approach has advantages like spatial resolution (due to large bandwidth), distance information, long range (lossless scatterer and low detection bandwidth), low cost (no semiconductor or printed electronics), ability to operate in non-continuous spectrum, potential to mitigate impairments (clutter, multipath) and interference and so on.

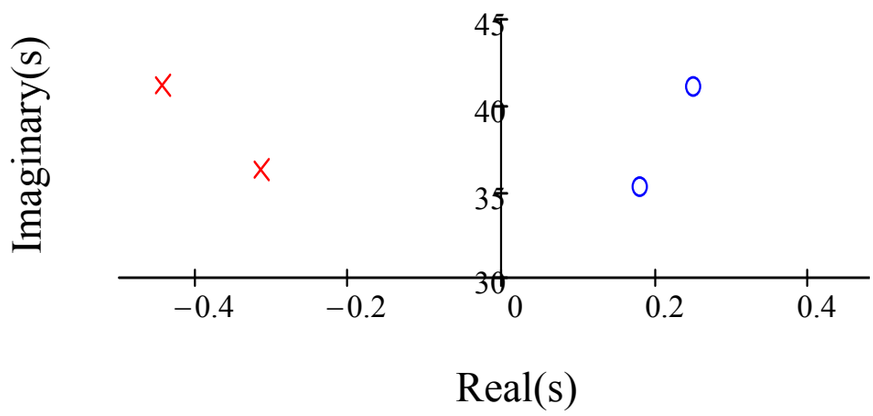

Fig. 14. Poles and Zeros of Stacked Microstrip Patches (Complex conjugate ones not shown)

The technique has the potential of providing sub-cent RF barcodes printable on low cost substrates like paper, plastic etc. It also has the potential to create sensors that directly convert a physical parameter to wireless signal without the use of associated electronics like Analog to Digital Converter, RF front-end etc.

To implement the approach, a category of antennas with certain specific properties has been identified. This type of antennas requires having low RCS with matched termination and constant RCS when terminated with a lossless reactance.

Next, a novel probing method to remotely measure impedance has been introduced. The method superficially resembles FMCW radar but processes signal differently.

Finally, a novel technique for the mitigation of impairments has been outlined. The mitigation technique is premised on the extraction of poles and zeros from frequency response data and separation of all-pass (target) from non all-pass (undesired) functions.

The work so far - based on mathematical analysis and computer simulation has produced encouraging results and therefore opens the path towards experimental verification.

There are certain areas that need further investigation e.g. development of various types of broadband 'all-pass' scattering structures with low structural scattering – or preferably, a general purpose synthesis tool to that effect. Another area is the development of broadband antennas that satisfy the scattering property mentioned earlier.

7. References

Andersen J.B. and Vaughan R.G. (2003) Transmitting, receiving and Scattering Properties of Antennas, *IEEE Antennas & Propagation Magazine*, Vol.45 No.4, August 2003.

Baev A., Kuznetsov Y. and Aleksandrov A. (2003) Ultra Wideband Radar Target Discrimination using the Signatures Algorithm, *Proceedings of the 33rd European Microwave Conference,* Munich 2003.

Balanis C.A. (1982) *Antenna Theory Analysis and Design*, Harper and Row

Bancroft R. (2004) *Microstrip and Printed Antenna Design*, Noble Publishing Corporation

Brunfeldt D.R. and Mukherjee S. (1991) A Novel Technique for Vector Measurement of Microwave Networks, *37th ARFTG Digest*, Boston, MA, June 1991.

Chauveau J., Beaucoudrey N.D. and Saillard J. (2007) Selection of Contributing Natural Poles for the Characterization of Perfectly Conducting Targets in Resonance Region, *IEEE Transactions on Antennas and Propagation, Vol. 55, No. 9, September 2007*

Collin R.E. (2003) Limitations of the Thevenin and Norton Equivalent Circuits for a Receiving Antenna, *IEEE Antennas and Propagation Magazine,* Vol.45, No.2, April 2003.

Dobkin D. (2007) *The RF in RFID Passive UHF RFID in Practice,* Elsevier

Hansen R.C. (1989) Relationship between Antennas as Scatterers and Radiators, *Proc. IEEE*, Vol.77, No.5, May 1989

Kahn W. and Kurss H. (1965) Minimum-scattering antennas, *IEEE Transactions on Antennas and Propagation*, vol. 13, No. 5, Sep. 1965

Mukherjee S. (2007) Chipless Radio Frequency Identification based on Remote Measurement of Complex Impedance, *Proc. 37th European Microwave Conference*, Munich, 2007

Mukherjee S. (2008) Antennas for Chipless Tags based on Remote Measurement of Complex Impedance, *Proc. 38th European Microwave Conference*, Amsterdam, 2008.

Mukherjee S., Das S.K and Das A.K. (2009) Remote Measurement of Temperature in Hostile Environment, *US Provisional Patent Application 2009.*

Nikitin P.V. and Rao K.V.S. (2006) Theory and Measurement of Backscatter from RFID Tags, *IEEE Antennas and Propagation Magazine*, vol. 48, no. 6, pp. 212-218, December 2006

Pozar D (2004) Scattered and Absorbed Powers in Receiving Antennas, *IEEE Antennas and Propagation Magazine,* Vol.46, No.1, February 2004.

Ulaby F.T., Moore R.K., and Fung A.K. (1982) *Microwave Remote Sensing, Active and Passive*, Vol. II, Addison-Wesley.

Ulaby F.T., Whitt M.W., and Sarabandi K. (1990) VNA Based Polarimetric Scatterometers¸ *IEEE Antennas and Propagation Magazine,* October 1990.

Yarovoy A. (2007) Ultra-Wideband Radars for High-Resolution Imaging and Target Classification¸ *Proceedings of the 4th European Radar Conference,* October 2007.

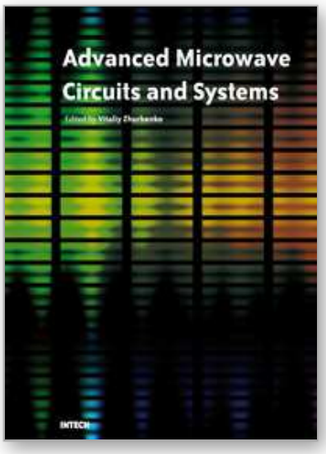

Advanced Microwave Circuits and Systems

Edited by Vitaliy Zhurbenko

ISBN 978-953-307-087-2

Hard cover, 490 pages

Publisher InTech

Published online 01, April, 2010

Published in print edition April, 2010

This book is based on recent research work conducted by the authors dealing with the design and development of active and passive microwave components, integrated circuits and systems. It is divided into seven parts. In the first part comprising the first two chapters, alternative concepts and equations for multiport network analysis and characterization are provided. A thru-only de-embedding technique for accurate on-wafer characterization is introduced. The second part of the book corresponds to the analysis and design of ultra-wideband low- noise amplifiers (LNA).

How to reference

In order to correctly reference this scholarly work, feel free to copy and paste the following:

Somnath Mukherjee (2010). Remote Characterization of Microwave Networks - Principles and Applications, Advanced Microwave Circuits and Systems, Vitaliy Zhurbenko (Ed.), ISBN: 978-953-307-087-2, InTech, Available from: http://www.intechopen.com/books/advanced-microwave-circuits-and-systems/remote-characterization-of-microwave-networks-principles-and-applications

INTECH
open science | open minds

InTech Europe
University Campus STeP Ri
Slavka Krautzeka 83/A
51000 Rijeka, Croatia
Phone: +385 (51) 770 447
Fax: +385 (51) 686 166
www.intechopen.com

InTech China
Unit 405, Office Block, Hotel Equatorial Shanghai
No.65, Yan An Road (West), Shanghai, 200040, China
中国上海市延安西路65号上海国际贵都大饭店办公楼405单元
Phone: +86-21-62489820
Fax: +86-21-62489821

© 2010 The Author(s). Licensee IntechOpen. This chapter is distributed under the terms of the Creative Commons Attribution-NonCommercial-ShareAlike-3.0 License, which permits use, distribution and reproduction for non-commercial purposes, provided the original is properly cited and derivative works building on this content are distributed under the same license.